CHAPTER-4

4.1. Introduction

In this chapter, Ba-Ce mixed metal oxide was emphasized as heterogeneous base catalyst in transesterification reaction for methyl esters production. The catalyst was characterized by sophisticated methods. *Millettia pinnata* oil was used as non-edible feedstock for methyl ester production. In this study, calcination temperature was optimized for synthesis of perovskite barium cerate with highest phase purity. Additionally, various Ba/Ce stoichiometric ratios were also checked to evaluate the active metal phase of catalyst. Ultimately, perovskite structure with 1:1 Ba/Ce was found to be most efficient one to catalyze the transesterification. This owed to the higher basicity value as well as compact and well-arranged perovskite crystal system which facilitated the catalysis on its surface. It produced the karanja oil methyl ester with 98.3±0.5% conversion at following experimental conditions: catalyst dose (1.2 wt %), oil to methanol molar ratio (1:19), reaction temperature (65˚C), reaction time (100 min), and agitation speed (600 rpm). The pseudo-first order kinetic model was again successfully established for transesterification reaction having activation energy (E_a) of 42.77kJ/mol. Furthermore, thermodynamics was also explored and important thermodynamic functions (ΔH°, ΔS°, and ΔG°) were reckoned using Eyring equation. The Environment-factor (E-factor) and turn over frequency (TOF) were enumerated as 0.088 and $21\times10^{-2}s^{-1}$. The physicochemical properties of the synthesized *Millettia pinnata* oil methyl esters were measured according to ASTM D 6751 and were found to be within the permissible range. It ensured the compatibility of produced methyl esters with existing CI engines without any further modification.

4.2. Catalyst synthesis

The catalyst was prepared using sol-gel polymer precursor or modified auto-combustion method (Maciel et al., 2003). The adequate amount of metal precursors was taken into the desired stoichiometric Ba/Ce ratio. The nitrate precursor of barium along with ceria was utilized for perovskite generation. The polymer precursor was produced from the alkaline earth metal precursor and citric acid. Ethylene glycol was incorporated to facile the polymerization reaction via extensive intermetallic network (Moghadam et al., 2013). The above mentioned aqueous solution was subjected to ultra-sonicated aqueous suspension of ceria with continuous agitation (350 rpm) for 2h at 60˚C. Onward, water was evaporated at 90˚C and then dried material was allowed to decompose at 350˚C to remove the organic moieties. Finally, the resultant grey powder was thermally treated at 1150˚C to acquire the stable metallic phase with no impurity.

4.3. Catalyst characterization

4.3.1. Thermal analysis

Thermo-gravimetric analysis (TGA) predicts the thermal stability of sample under high-temperature conditions. The differential thermo-gravimetric (DTG) curve is derived from the first derivative of the TG curve and informs about degradation rate through sharp peaks. It gives a clear picture of temperature range onto mass loss is drastic while differential thermal analysis (DTA) predicts about either endothermic or exothermic phase transitions. Thermal behavior of prepared barium cerate (Ba/Ce with 1:1) sample can be explained by TGA/DTA/DTG curve as in Figure 4.1. As it can be easily seen, there is no exothermic or endothermic transition in DTA except three consecutive thermal degradation steps in TGA. The mass losses are not very drastic or acute rather they cover a temperature range from ambient to 1150˚C while gradual

mass degradation. A very small peak in DTG curve at ambient temperature (40˚C) manifests a flat loss in TGA up to 200˚C which generally belongs to the moisture removal from the catalyst (Singh et al., 2016). The mass loss of 4.08 % in the thermal curve (Figure 4.1) represented at 363˚C in DTG owes to desorption of hydroxyl followed by nitrate degradation from catalyst surface during synthesis. These two back to back slow mass losses from 400˚C to 800˚C and from 850˚C to 1100˚C correspond to the total mass loss of 14.51 %. The second flat mass loss in TGA, right from 400˚C-800˚C is related to the decomposition of nitrate and residual organic impurities from citric acid and ethylene glycol left (Atadashi et al., 2013). This may stand to the beginning of reaction between resultant intermediate $BaCO_3$ and solid CeO_2.

$$BaCO_3 + CeO_2 \longrightarrow BaCeO_3 + CO_2 \qquad (4.1)$$

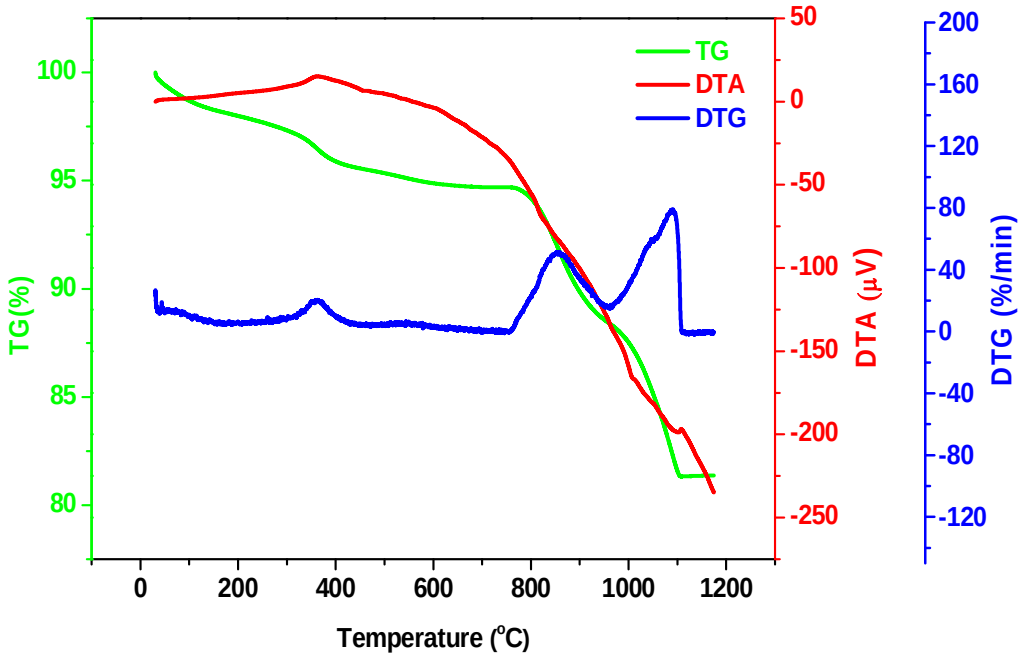

Figure 4.1 Thermal curves of crude catalyst.

This is the sole process in 1:1 metal stoichiometric ratio but non-stoichiometric ratio forms metal native oxide. The last peak shown in the DTG curve in the range of

800˚C to 1100˚C is attributed to residual metal carbonate degradation (Lee et al., 2014). Though barium carbonate is very thermo-stable and not easily degradable, it ends with the slow reduction process till a high temperature (Atadashi et al.,2013; Lee et al.,2014; Sahani and Sharma, 2018). After the detailed thermal analysis, calcination temperature was optimized at 1150˚C for 3.5h. At this temperature, the desired phase appeared with least impurity.

4.3.2. Powder XRD analysis

XRD analysis was made to check the phases formed within the crystal lattice. The prepared perovskite structure was confirmed by phase analysis. The diffractogram in Figure 4.2(a) manifested the prominent peaks corresponding to only orthorhombic perovskite formula of $BaCeO_3$ after matching it with JCDPS file no #822425 (Venkatasubramanian et al., 2010; Kumar et al., 2017). The major peaks positioned at 28.7˚ (002), 40.9˚ (022), 50.8˚ (213), 59.4˚ (004), 67.2˚ (611), and 74.6˚ (404) got matched with prominent peaks in XRD diffractogram (Kumar et al., 2017). After the synthesis of crude catalyst, calcination time was inspected for the maximum phase stability and purity. Highest intensity peaks show its crystalline nature with the least impurity. It was found from Figure 4.2(d) that with duration of 2h the metal carbonates phase is evolved as the peaks with the highest intensity at 19.4˚ (110), 23.9˚ (111), and 27.7˚ (002) are easily visible so it could be diminished if treatment time is raised (Basahel and Diefallah, 1992). The pure perovskite phase was observed without those earlier mentioned peaks assuring the absence of metal carbonate species. As the enhancement in calcination time facilitated the carbonate degradation, peaks corresponding to metal carbonates started to disappear from diffractogram as in Figure 4.2. After formation of the perovskite structure, active phase of the two metal

combinations was explored by altering the metals stoichiometry within crystal lattice such as three combinations were synthesized with 1:2, 1:1 and 2:1 Ba/Ce ratio. These prepared samples were also gone through XRD analysis showing their crystal structure through constructive diffractions resulting corresponding peaks in diffractogram.

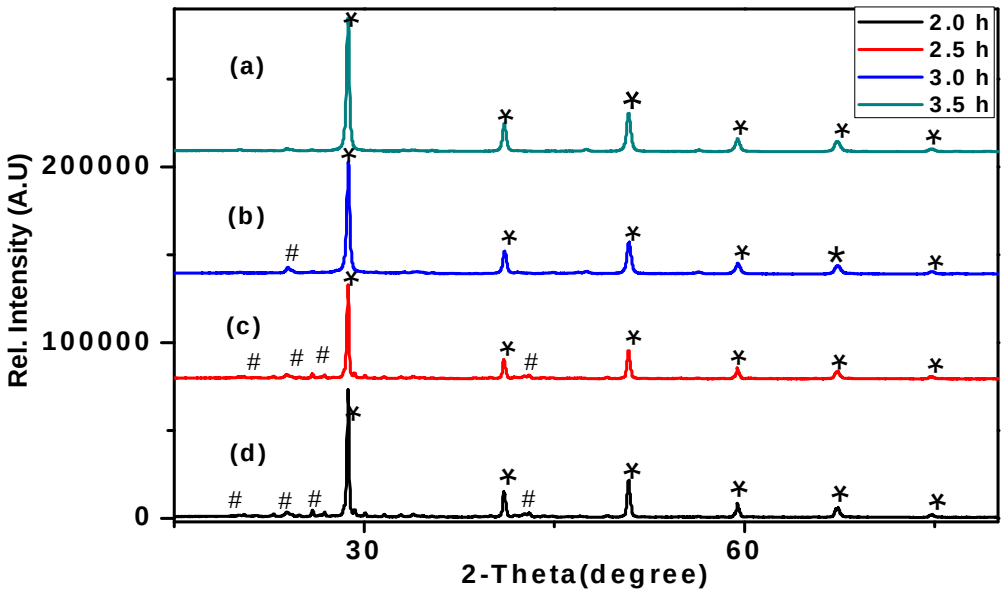

Figure 4.2 XRD diffractogram of perovskite sample calcined for different time intervals.

Figure 4.3 represents the different phases formed in all three samples with their nomination in diffractogram. The perovskite structure is retained as its structural formula suggests the Ba/Ce in 1:1 proportion in Figure 4.3(c). Only peaks attributed to this structure are available with no other parallel existing phase. But in Figure 4.3(b), excess Ce atoms form their native oxides (Valechha et al., 2011) along with anticipated perovskite formula and further confirmed by the presence of peaks at 28.6˚ (111), 33.5˚ (200), 47.3˚ (220), 56.8˚ (311), 59.3˚ (222), 69.4˚(400), 76.2˚(331), 79.7˚(420) got matched with JCPDS file #655923. At last, the XRD diffractogram in Figure 4.3(a)

contains several peaks specified multiple phase formations. As barium finds its great philicity towards carbonate and it is not easily decomposed even at 1150˚C once it exceeds after the balanced Ba/Ce stoichiometry of 1:1. Due to partial decomposition barium carbonate still existed and made its presence in diffractogram with prominent peaks at 19.9˚ (110), 23.9˚ (111), 27.7˚ (140), 33.4˚ (200), 34.1˚ (112), 42.0˚ (221), 44.1˚ (132), 43.8˚ (113), and 56.3˚ (151) mentioned in JCPDS file #712394 (Sahani and Sharma, 2018). The other mild peaks are of low intensity and comparatively not visible. The other prominent phase is $BaCeO_3$ as the peaks related to this phase are present with significant intensity. Native oxide formation is quite ambiguous as the peaks related to either CeO_2 and BaO are superimposed with other existing phases (Mohadesi et al., 2014; Khedr et al., 2014). Only above mentioned two phases are in majority in crystal lattice which was further confirmed by FT-IR analysis.

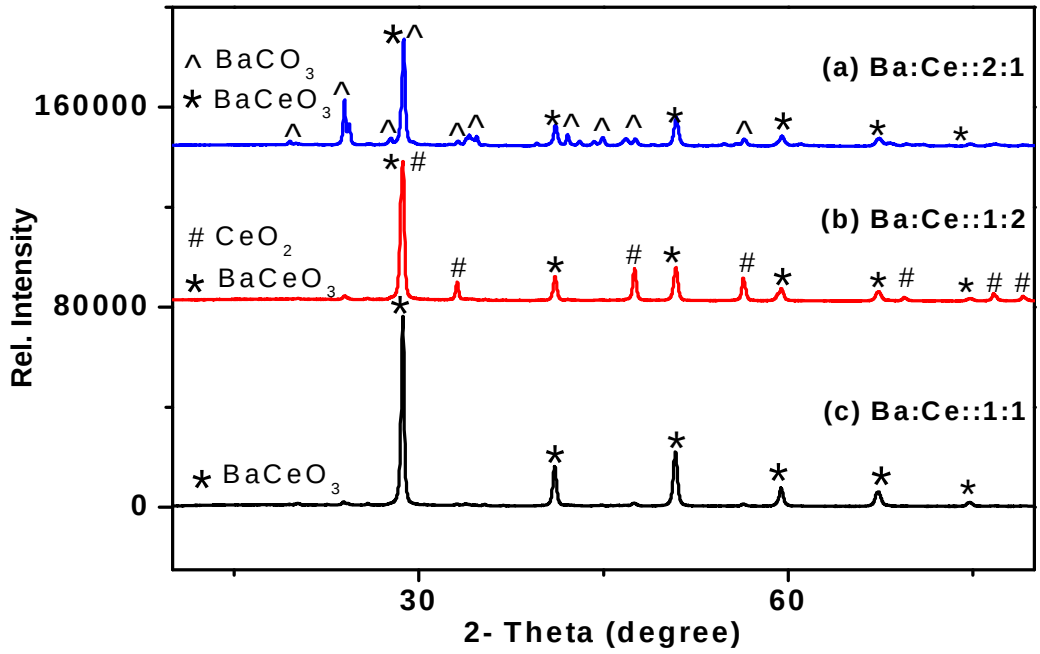

Figure 4.3 XRD diffractogram of calcined catalysts with Ba/Ce stoichiometric ratio.

4.3.3. Surface morphological analysis

The SEM image of the fired powder (Figure 4.4(a)) comprised of agglomerates of bimodal CeO_2 particles and intermediate species of barium after decomposition at 350˚C might be of $BaCO_3$. This might be attributed to mall-functioning of uncalcined material as it did not offer any sort of catalytic activity. Especially, the untreated catalyst is filled with carbonate species making it highly acidic which is completely undesirable for transesterification. Comparatively, perovskite structure seemed to be compact and finer in size depicted in Figure 4.4(d). Native metal oxides formed bulkier particles exposing least area as active site for reaction.

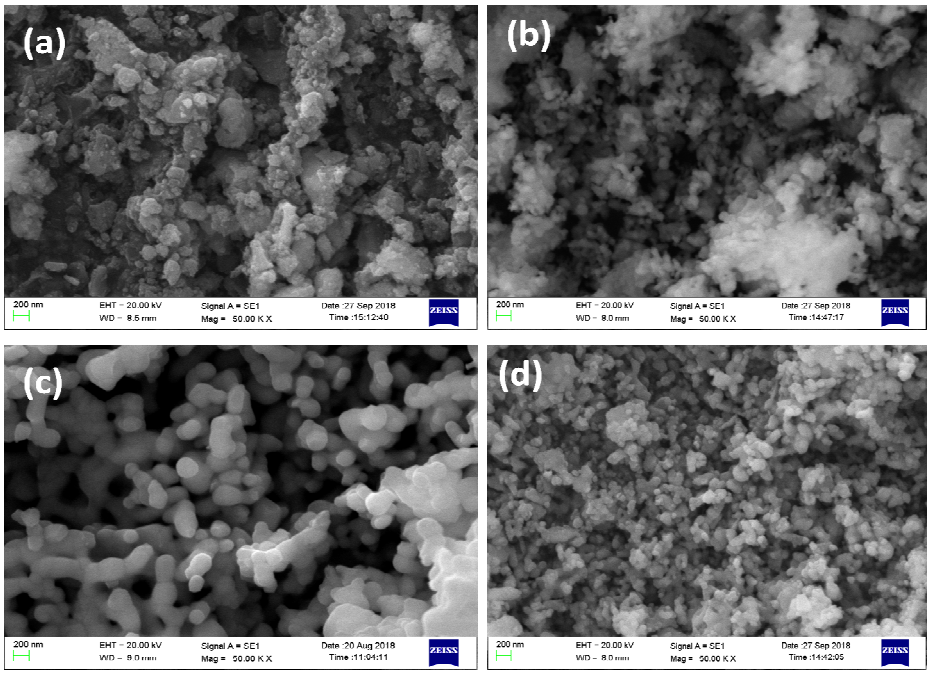

Figure 4.4 SEM image of synthesized catalyst; (a): uncalcined perovskite sample, (b): Ba/Ce: 2/1,(c):Ba/Ce: 1/2, (d) Ba/Ce: 1/1(perovskite).

Smaller sized and uniformly assorted particles favored the perovskite structure to be active for transesterification. The formation of native metal oxides resulted in different crystal structures having particle size over a range of length with as in Figure

4.4(c). The catalyst sample having $BaCO_3$ traces with the perovskite structure and bare metal oxide adsorbing carbonate clusters can be easily seen in Figure 4.4(b). The particle size of the perovskite sample was calculated with the help of Image J software and found to be in a range of 80 to 120nm which revealed perovskite $BaCeO_3$ as nanocatalyst. Barium cerate acquired the perovskite with Ba/Ce as 1:1 was crosschecked by Elemental composition analysis (EDS) (Figure 4.5) including both atomic% and weight% of all three elements in barium cerate. The results obtained from EDXS substantiated the predicted 1:1 Ba/Ce stoichiometry in perovskite $BaCeO_3$.

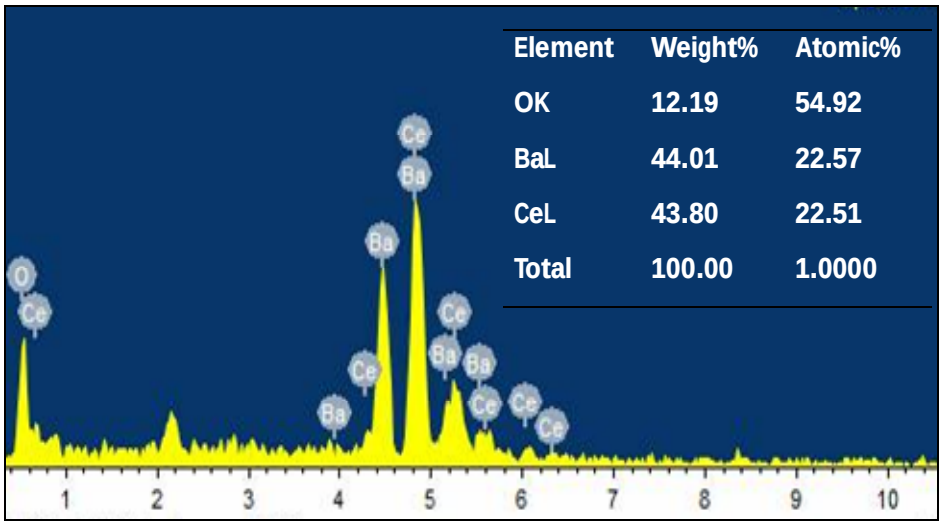

Figure 4.5 EDXS histogram of perovskite catalyst.

4.3.4. FT-IR analysis

FT-IR analysis was conducted to elaborate the nature of functional groups within catalyst lattice to explain the metal oxide bonding to back the finding from XRD analysis. The FT-IR spectra covered the entire range of IR comprising both the functional and the fingerprint region (4000 cm^{-1} - 500 cm^{-1}). The perovskite structure with homogeneous phase was confirmed in Figure 4.6(e). As it is quite clear from Figure 4.6(e) that only M-O-M' bond peak is with the highest intensity at 529cm^{-1} (Berbenni et al., 2001; Brzozowski and Castro, 2003). Another broad peak around 3740

cm^{-1} with mild intensity indicates the presence of areal moisture. A fine comparison is made between thermally untreated catalysts with that of calcined one for 3.5h. Because further increment in calcination time did not accommodate any change in spectra as the desired phase was achieved during this much calcination time. Right in Figure 4.6(a), it can be easily seen that the individual $BaCO_3$ structure is coexisting with perovskite structure with intense peaks at 857cm^{-1}, 683 cm^{-1}, 857 cm^{-1}, 1069 cm^{-1}, 1429 cm^{-1}, and 1750 cm^{-1}(Waal et al., 1998; Vahur et al.,2016). The areal CO_2 has also shown its presence at 2350 cm^{-1} (Boschini et al.,2003). During calcination, organic moiety with carbonate species got removed from catalyst which pacified the interphasic insertion between native oxides to form $BaCeO_3$.

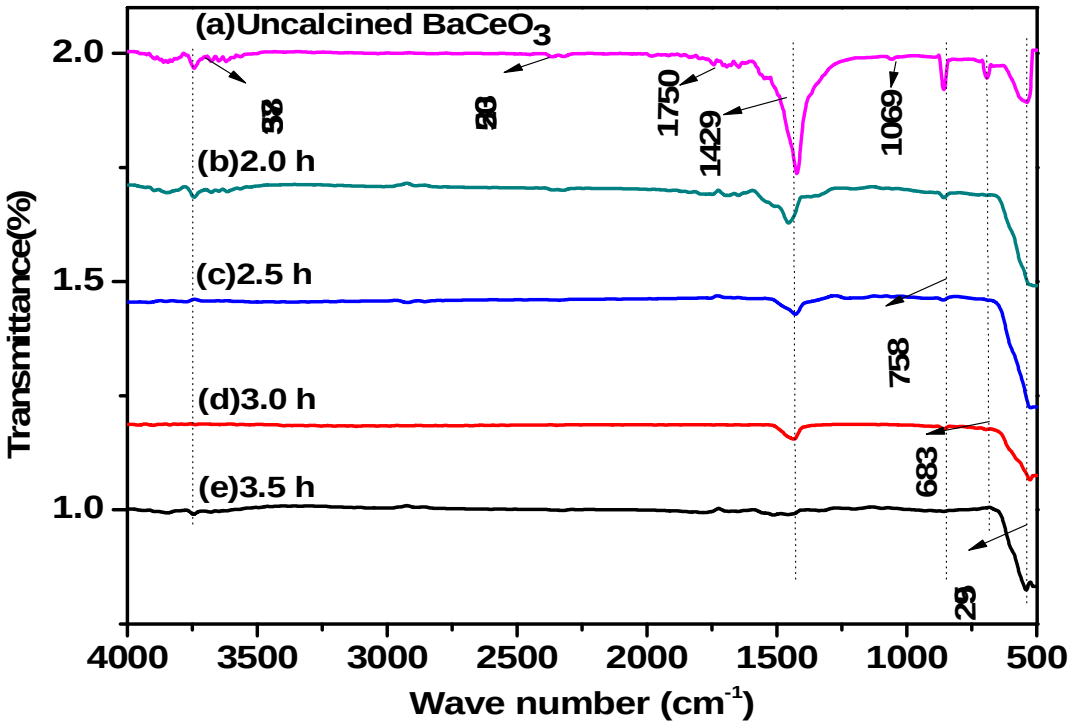

Figure 4.6 FT-IR spectra of perovskite material calcined at different time interval.

Now, Figure 4.7 demonstrates the FT-IR spectra of catalyst samples with different Ba/Ce stoichiometry of 2:1, 1:1, and 1:2 proportions. The spectra including different samples contain the prominent transmittance peaks regarding specific M-O-M

bonds owing to stretching frequencies of all major functional groups present in samples. The high intensity but broad peak at 1429 cm^{-1} represents the metal carbonate which has been vanished in Ba/Ce with 1:1 in Figure 4.7(b). As in Figure 4.7(c), Ba/Ce 2:1 stoichiometrically excess Ba has formed its carbonate which is reflected in FT-IR spectrum having peaks at 683 cm^{-1}, 868 cm^{-1},1429 cm^{-1}, 1748 cm^{-1}, 2452 cm^{-1} (Shahid et al., 2018) with the extent of adsorbing water appeared around 3700 cm^{-1}. In case of 1:2 where an excess of CeO_2 has been stipulated during synthesis remained as CeO_2 which has been identified by FT-IR spectra in Figure 4.7(a) by reflecting a shoulder peak at 1380 cm^{-1} and a prominent peak at 521cm^{-1} (Bai et al., 2014; Farahmandjou et al., 2016) superimposed with high-intensity peaks attributed to perovskite structure.

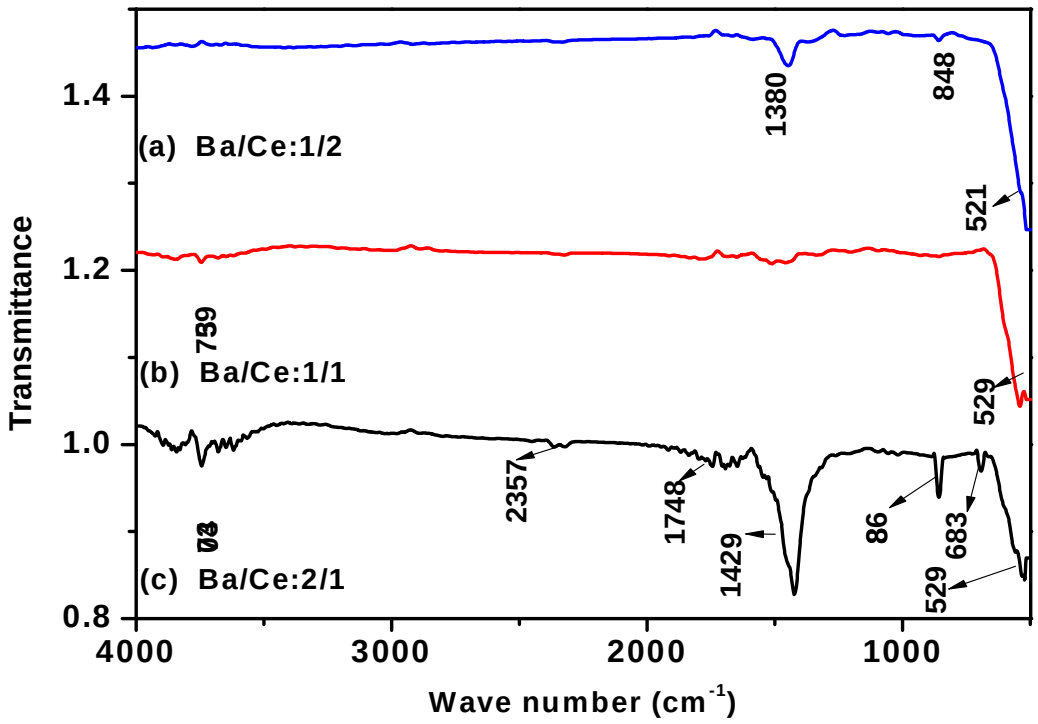

Figure 4.7 FT-IR spectra of calcined catalysts with different Ba/Ce stoichiometric ratio.

4.3.5. BET surface area analysis

Basicity of the prepared perovskite structure was determined by BET analysis. This informed the extent of the available adsorbent sites for approaching reagents. The BET surface area analysis substantiates the SEM information showing the catalytic ability owing to the highest BET surface area (32.31 m^2/g) as well as compatible pore size (7.33 nm) well suitable for co-interaction between triglyceride and adsorbed methanol on catalyst (Sahani and Sharma, 2018).

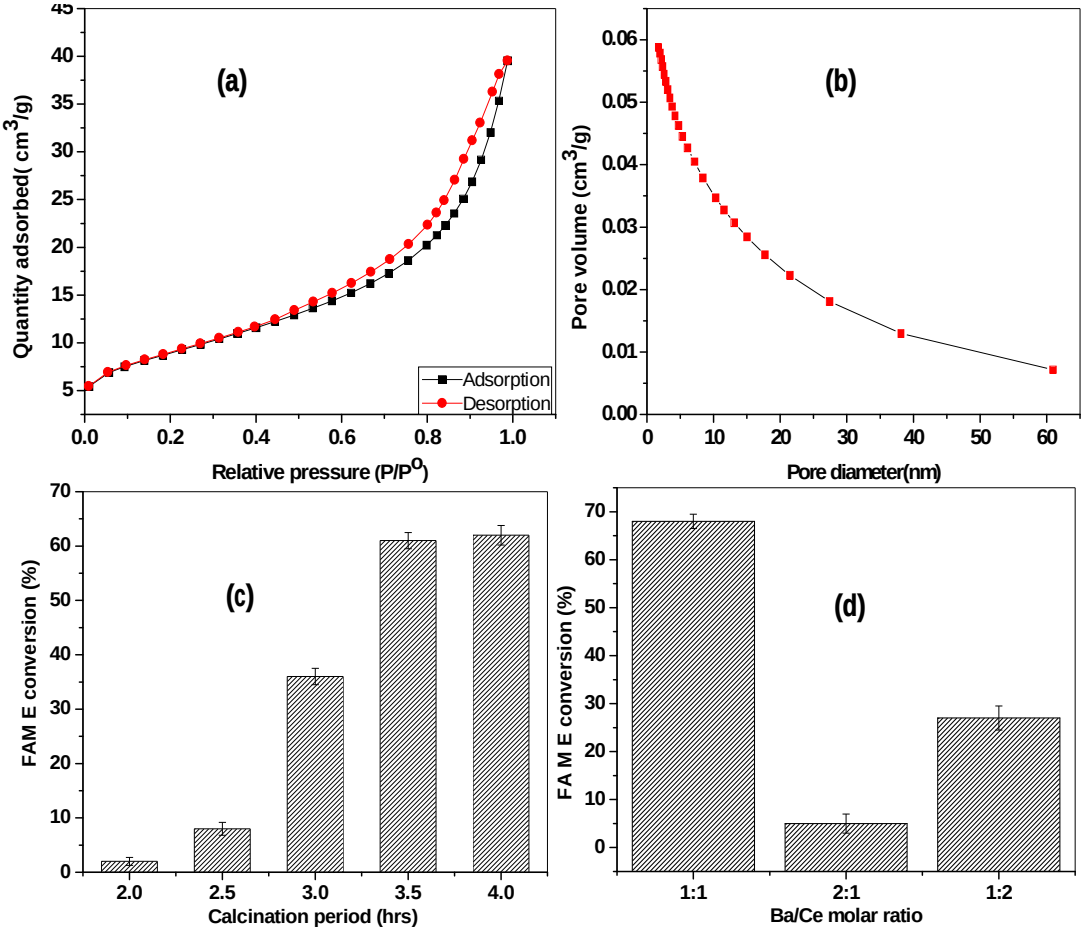

Figure 4.8 a) N_2 adsorption-desorption isotherm (BET) linear plot; (b) BJH adsorption cumulative pore volume; (c) optimization plot of calcination period for perovskite synthesis ;(d) plot inferring the metals stoichiometric ration on FAME conversion.

It is also noted that exposed area for surface catalysis is maximum in perovskite catalyst (Ba/Ce with 1:1) in comparison to other catalyst samples with different Ba/Ce stoichiometric ratio. This also might be reason for its highest catalytic efficiency in transesterification reaction. The pore size distribution of $BaCeO_3$ was found in the range of 2-50 nm which classified the catalyst as mesoporous material. The isotherm profile of IV type validates pore size distribution analysis regarding hysteresis type III, being characteristic of mesoporous materials **(Moura et al., 2016)**. The hysteresis at high pressures is consistent with uniform and one-dimensional pores present in perovskite catalyst.

4.3.6. Basicity

This heterogeneous catalysis is mainly governed by two major parameters i.e. surface area and basicity. The synergistic effect of both the parameters impacts the transesterification. In order to calculate basicity, several indicators as discussed above were taken into account for the reliability of results. On the basis of several Hammett titrations, a concrete basicity of barium cerate was evaluated to be 1.74mmol/g. This basicity value is fair enough than many barium based catalysts which are previously reported in the literature (Singh et al., 2016).

4.4. Effect of calcination time for $BaCeO_3$ synthesis and different Ba/Ce stoichiometric ratio on FAME conversion

It incorporates the effect of Ba/Ce stoichiometric ratio and calcination time with respect to transesterification reaction. Initially, the desired perovskite structure was verified by X-ray diffractogram (Figure 4.2) and FT-IR (Figure 4.6). An optimization was implemented to achieve the proper calcination interval at following preliminary

reaction conditions in Figure 4.8(c): oil to methanol molar ratio (1:15), catalyst dose (1.5wt%), reaction temperature (55˚C), reaction time (2h) and agitation speed (500 rpm). The uncalcined catalyst could not facile the FAME conversion as it did not consist of the catalytically active phase but calcination at appropriate temperature created the catalyst with the pure perovskite structure which finally caused the highest methyl ester transformation in 3.5 h. After that, conversion got stabilized as the catalyst with pure $BaCeO_3$ was formed and supposed to be the most active phase responsible for O-H bond cleavage in methanol to produce acyl acceptors. Afterwards, selection of perfect metals stoichiometry was explored by varying the molar ratio of both metals. The Ba/Ce with 1:1 was found to be the best candidate because of its active perovskite phase in Figure 4.8(d). The problem with 1:2 Ba/Ce is beside the formation of $BaCeO_3$, there is the formation of separate CeO_2 confirmed by XRD and FT-IR which is not the active phase and does not contribute towards catalysis in transesterification (Zhang et al., 2018). In case of 2:1 Ba/Ce, the prepared catalyst $BaCeO_3$ loses its catalytic activity due to presence of $BaCO_3$ confirmed by both XRD and FT-IR having acidic sites nullifying the basic character necessary for CH_3O^- generation during reaction mechanism.

4.5. Effect of process variables on FAME conversion

4.5.1. Effect of oil to methanol molar ratio and catalyst dose

These two effects are known to be the most important factors playing the key role in transesterification. As the reaction between ester and alcohol is quite reversible, it requires an excessive amount of alcohol than the stipulated amount from the stoichiometrically balanced equation (Balat and Balat, 2010; Arora et al., 2014). According to Lee Chateleir's principle, equilibrium continues in that direction where

stress can be relieved (Balat and Balat, 2010). So, the transesterification can be dragged towards product side with an excess of methanol. Here, the optimum oil to methanol molar ratio was found out to be 1:19 which was comparatively higher than stoichiometric ratio. This might be owing to the higher viscosity of non-edible karanja oil (Lee at al., 2014). Therefore, higher oil to methanol molar ratio (1:19) resulted in greater methyl ester conversion in lesser time. After achieving the equilibrium, excess methanol started dissolving the glycerol, the byproduct making its separation quite cumbersome and also made purification process more difficult. The excess methanol with its hydroxyl group could behave as an emulsifier, thus formed emulsified medium tougher to separate (Dai et al., 2015). This theoretical basis was exactly followed by reaction mechanism and can be grasped from optimization plot in Figure 4.9(a).

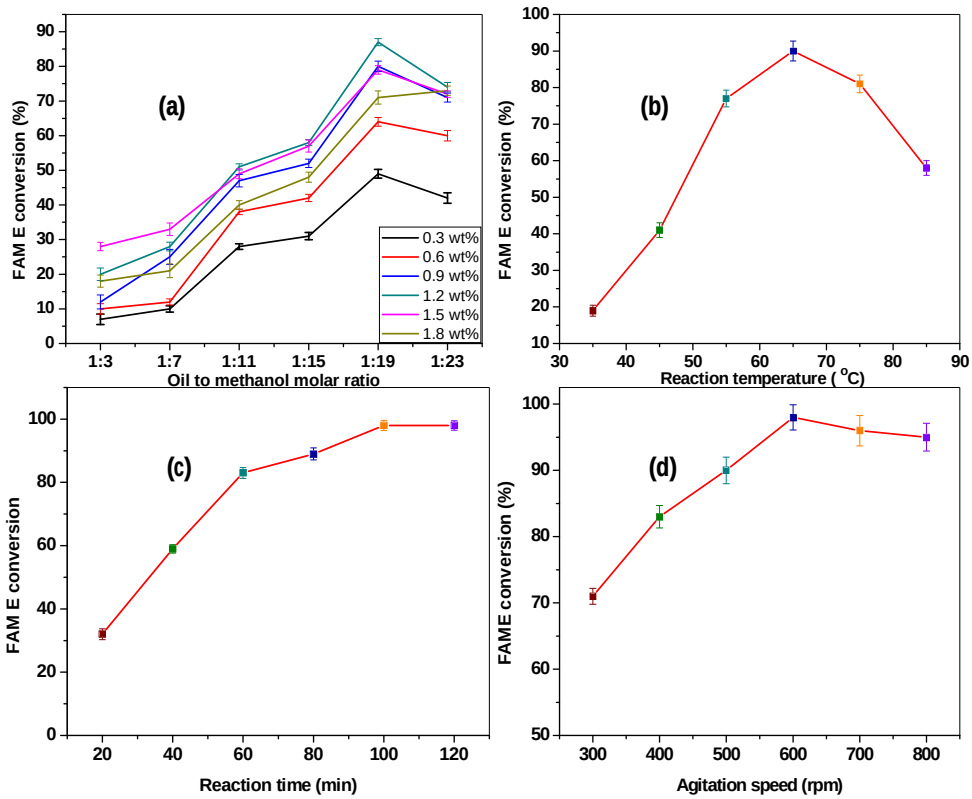

Figure 4.9 Optimization plots showing the impact of various process variables on KOME conversion (a) synergistic effect of catalyst dose with oil to methanol molar ratio;(b) reaction temperature;(c) reaction time;(d) agitation speed.

The catalyst dose plays an important role as catalyst surface has the highest significance as it provides its surface for the methanolysis (Likozar and Levec, 2014) for further processing of transesterification. Reaction system must have the sufficient amount of active sites to facile the generation of CH_3O^- simultaneously to meet up the triglyceride molecules. Subsequently, this CH_3O^- approaches to triglyceride and accepts acyl from TG and form methyl ester. As it can easily be interpreted from Figure 4.9(a), the reaction is accelerated in the presence of a catalyst to an optimum extent here i.e. 1.2 wt %. Beyond that reaction was disfavored as catalyst concentration started playing the negative role because of increased fluid viscosity in the reaction system which disrupted the interactions between reactant molecules.

4.5.2. Effect of reaction temperature

Many reports registered reaction temperature as a key process variable which governed the kinetics of any chemical reaction (Sharma et al., 2011a; Dai et al., 2015). The optimum temperature was deduced by conducting several batch wise transesterification reactions over a range of temperature right from the ambient temperature to the temperatures even higher than boiling temperature of methanol. Here, optimum temperature provides the sufficient energy trespassing with the required threshold to cross the reaction coordinate in the forward direction. The highest reaction yield was attained near the boiling temperature (BT) of methanol used. Around the BT of methanol, acyl acceptor generated from methanol had attained the threshold energy to approach the triglyceride and formed the methyl ester. Above 65˚C, methanol got evaporated and left the boundary of the triphasic reaction system. As a result, methanol lost its contact with triglyceride and lowered methyl ester production. This assertion was also stated by profile obtained in Figure 4.9(b). Here, the profile signified that

there was a drastic 2 to 3 fold increase in ester conversion as the temperature raised from ambient to an optimum temperature. This might be attributed to the kinetic factor which has been already discussed above (Balat and Balat, 2010).

4.5.3. Effect of reaction time

Reaction time is supposed to be most important governing parameter which drives the reaction kinetics (Balat and Balat, 2010). The reaction time was extended to 2 h at 65˚C using 1.2 wt % catalyst dose to check the completion time in order to get highest methyl ester conversion. As it is seen from Figure 4.9(c), initial one hour produced more than 80% of methyl ester. In first 10 min, the reaction could not make any significant amount of KOME as the reaction was diffusion controlled. Once, the kinetically controlled phase was about to approach, reaction rate got amplified and produced more methyl ester (ME) shown by time profile. After equilibrium phase, reaction got slowed down and finally achieved saturation in 100min. Beyond optimum reaction time, ester hydrolysis might have begun and reduced the ME conversion (Singh et al., 2016).

4.5.4. Effect of agitation speed

The last but not the least, the agitation speed does also control the fate of reaction to significant extent (Likozar and Levec, 2014). As the reaction system is heterogeneous with three distinct phases, there must be proper mixing to allow the contact among reacting molecules. When agitation was too slow, KOME conversion was not enough because of improper contact among reactants. Agitation speed was optimized at 600 rpm (Figure 4.9(d)), while faster agitation mitigates the appropriate contact time which is mandatory for the reactant species to turn out into the product. One more thing might be causing loss of ME conversion that swifter agitation may

cause the evaporation of methanol (having the low boiling point, mind it that reaction system got its maximum at around 65˚C; very near to BT of methanol) (Likozar and Levec, 2014). At the end of the optimization process, the highest (>98%) FAME conversion was resulted in $BaCeO_3$ catalysed transesterification.

4.6. Kinetic and thermodynamic studies

In current study, the experimental data were interpreted over a span of reaction time at different reaction temperatures (308 K, 318K, 328 K, and 338 K). The kinetic plot in Figure 4.10(a) exhibits the rational linearity anticipating the model of pseudo first order kinetics. Furthermore, the rate constants at 308 K, 318 K, 328 K and 338 K were determined to be 8.4×10^{-3} min^{-1}, 1.2×10^{-2} min^{-1}, 1.6×10^{-2} min^{-1} and 3.1×10^{-2} min^{-1}, respectively.

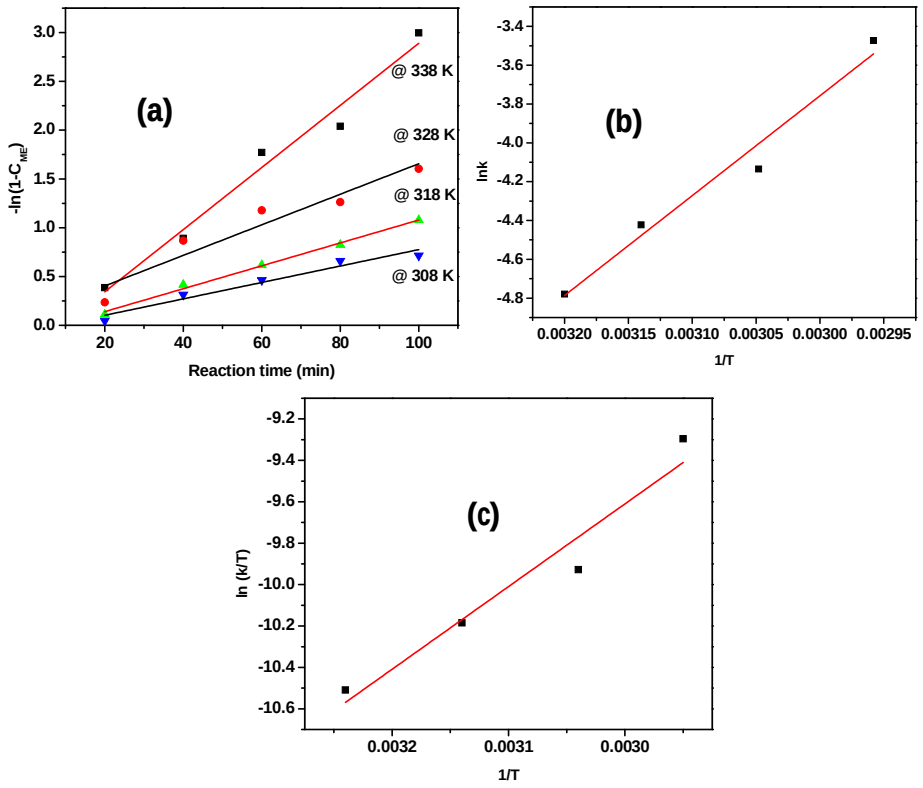

Figure 4.10 (a) -ln (1-C_{ME}) versus reaction time (min) plot at different temperatures using most optimized conditions, (b) Arrhenius plot lnk versus 1/T (K^{-1}) for KOME synthesis from its crude oil,(c) Eyring plot.

The experimentally derived rate constants support the outcomes that higher temperature accelerates transesterification process owing to promoted mass transfer. The activation energy (E_a) and pre-exponential factor were determined as 42.77kJ mol^{-1} and $11.94\times10^{4}min^{-1}$ respectively. The activation energy (E_a) lies in the range of 33.6-84kJ mol^{-1} which regards to activation energies for base-catalyzed transesterification reactions mentioned in the literature (Lee et al., 2014; Sahani and Sharma, 2018, Moura et al, 2016). From Figure 4.10(c), values of ΔH^o and ΔS^o were computed and found to be 33.21 kJ/mol and -177.99J/mol, respectively from the linear plot of Eyring equation i.e. ln (k/T) versus 1/T. The positive value of ΔH° deduced the endothermic nature of transesterification reaction which meant that the external energy supplement was needed for the transformation of reactants to products via in between generation of activated complex (Banerjee et al., 2019), whereas the negative value of ΔS° value was the indication of deduction in system randomness. Ultimately, ΔG° values were assessed to be 88.04 kJ/mol, 89.82 kJ/mol, 91.60kJ/mol, and 93.38kJ/mol at 308 K, 318 K, 328 K and 338 K respectively. The positive ΔG° values asserted the non-spontaneity of the transesterification reaction at any chosen temperature even at most optimized temperature condition (Banerjee et al., 2019; Roy et al., 2019).

4.7. Reusability test and leaching studies

The application of heterogeneous catalysis is preferred over homogeneous one because of its endurance capacity (Singh et al., 2016). The endurance capacity of perovskite material was diagnosed by regenerating it after each cycle. Catalyst regeneration was performed by multiple washing with ethanol and methanol subsequently and then it was calcined at 600˚C. This caused the removal of reversible deposition of adsorbents. This let the prepared catalyst find its reusability till sixth

cycles with KOME conversion capacity greater than 81% (Figure 4.11).

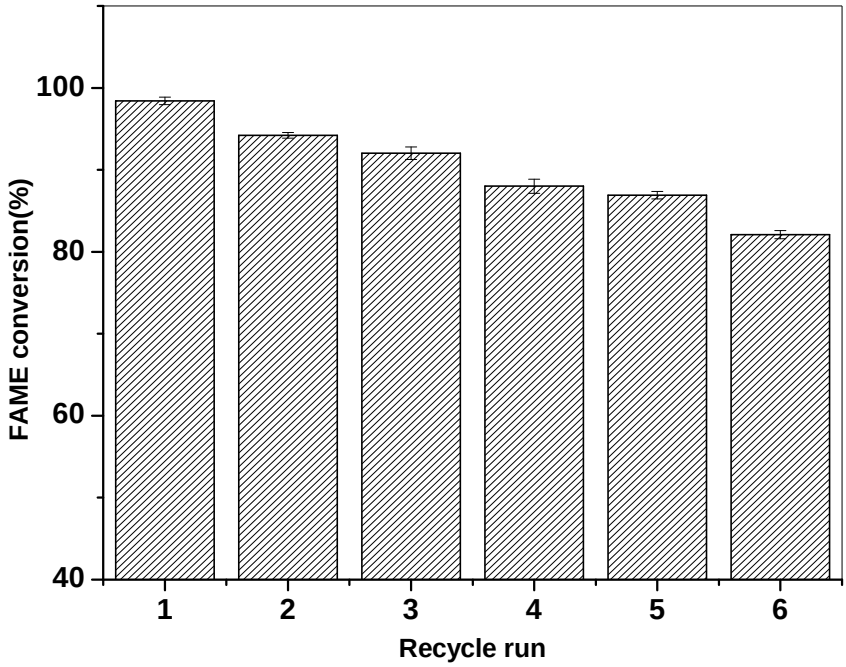

Figure 4.11 Reusability test of perovskite catalyst.

However, catalyst lost its efficiency due to irreversible catalytic poisoning say surface passivation through pore clogging by organic residues extracted from feedstock during transesterification while multiple recycling (Sahani and Sharma,2018). The surface adsorption of nuisance groups such as carbonate species derived from organic molecules sustained even after regeneration process. This feasible phenomenon was also supported by FT-IR analysis (Figure 4.12). This reduced the basicity of catalyst and further assuaged the FAME conversion in transesterification reaction. In Figure 4.12, an intense and broad peak at 1480 cm^{-1} reflects the irreversible accommodation (Sahani and Sharma, 2018) of carbonate species extracted from organic residues on the outer boundary of the catalyst. This characteristic peak in $BaCeO_3$ at 521 cm^{-1} got broadened owing to deformation of its exclusive perovskite structure.

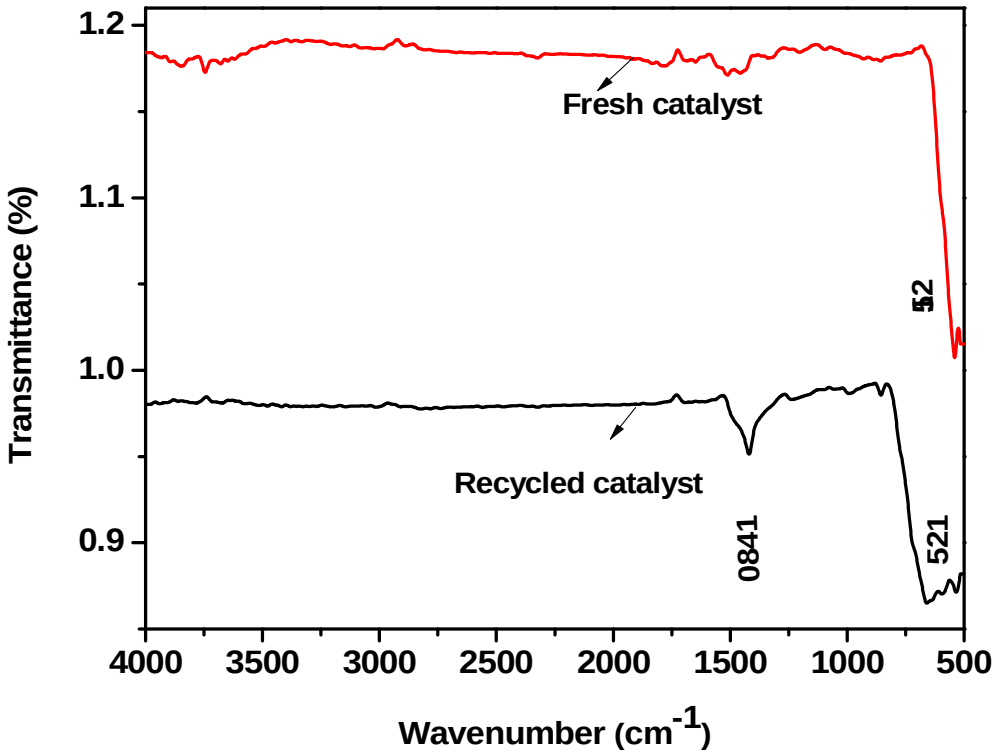

Figure 4.12 FT-IR spectra for comparative study of fresh barium cerate and recycled catalyst.

4.8. E-factor and TOF

E-factor is calculated and found to be 0.088 which indicated that the heterogeneous basic catalysed transesterification reaction to be a green approach for a cleaner biodiesel production. TOF for KOME formation through transesterification reaction using $BaCeO_3$ was calculated to be 21×10^{-2} s^{-1}. This finding shows the close agreements with results demonstrated in literature (Emin and Erol, 2012; Moura et al, 2016). The insignificant E-factor and appreciable TOF values propose the $BaCeO_3$ as a sustainable and potential solid catalyst for greener transesterification reaction.

4.9. Methyl ester characterization

4.9.1. GC-MS

The chemical composition of feedstock was ascertained by GC-MS analysis.

Gas chromatogram of methyl ester derived karanja oil has been featured in Figure 4.13.

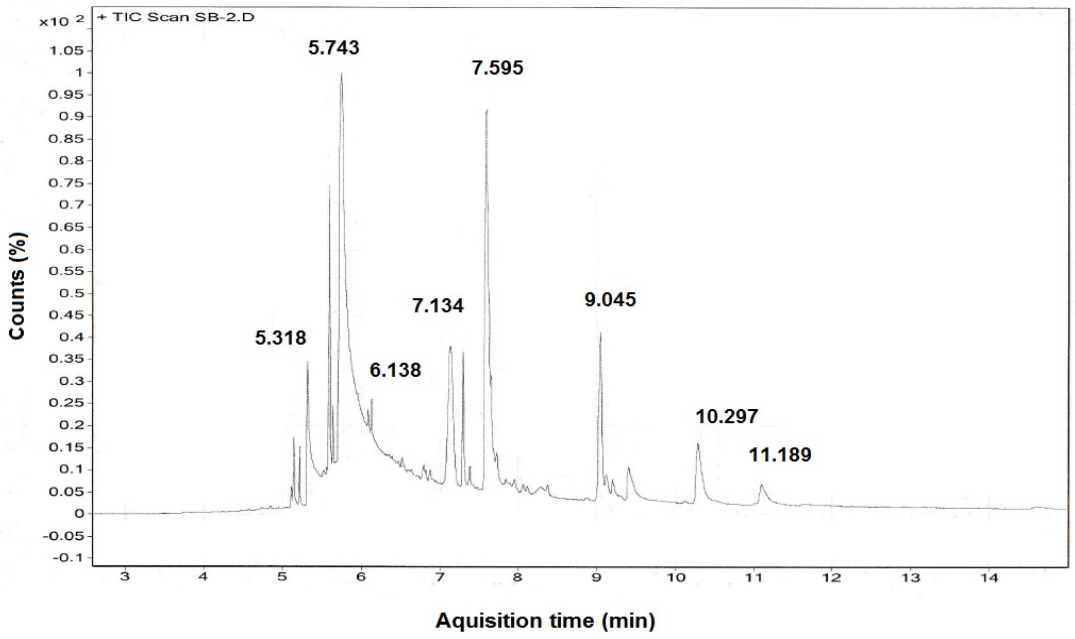

Figure 4.13 GC-MS profile of fatty acid methyl ester derived from *Milletia pinnatta* oil.

Mass spectrum regarding each component in GC was interpreted using NIST database. It is concluded that feedstock primarily constitutes unsaturated fatty acid. GC-MS of fatty acid methyl ester confirmed the presence of five major fatty acids enlisted in Table 4.1. The total sum percent of unsaturated fatty acid content exceeds more than 75% of entire composition. The oleic acid came out to be the most prominent unsaturated fatty acid component in GC-MS profile (Vivek and Gupta, 2004).

Table 4.1

Fatty acid composition of fatty acid methyl ester derived from *Milletia pinnatta* oil obtained from GC-MS.

S. No.	Retention time (min)	Corresponding fatty acid	No of Cs: d.b.	Area sum (%)
1	5.318	Dodecanoic acid	C_{12}:0	6.28
2	5.743	9-octadecenoic acid	C_{18}:1	43.21
3	6.138	cis-10-Heptadecenoic acid	C_{17}:1	13.26
4	7.134	Cis,9-12-octadecenoic acid	C_{18}:2	1.73
5	7.595	Octadecanoic acid	C_{18}:0	22.25
6	9.045	Nonadecanoic acid	C_{19}:2	8.03
7	10.297	Pentadecanoic acid	C_{15}:1	3.24

4.9.2. ^{1}H-NMR and ^{13}C-NMR

The fatty acid methyl ester from *Milletia pinnatta* oil was analyzed by ^{1}H-NMR spectroscopy which has been shown in Figure 4.14(a). The quantification of methyl ester conversion was executed through ^{1}H-NMR analysis and 98.3% FAME conversion was achieved. The characteristic signal attributed to methoxy protons in FAME appeared as a singlet at δ3.68 ppm. The triplet signal at δ 2.30 ppm was related of α-CH_2 protons of ester (Madhu et al., 2017). The stretching vibration corresponding to α-CH_2 across carbon double bond positioned as multiplet around δ 2.03-2.07ppm. A multiplet at δ 1.61-1.63 ppm displayed the presence of β-methylene protons in methyl ester. The high intensity signals at δ 1.26 and δ 1.31 ppm exhibited the backbone methylene protons of fatty acid moiety. The terminal methyl protons of carbon chain in fatty acid were observed as multiplet at δ 0.86-0.89 ppm.

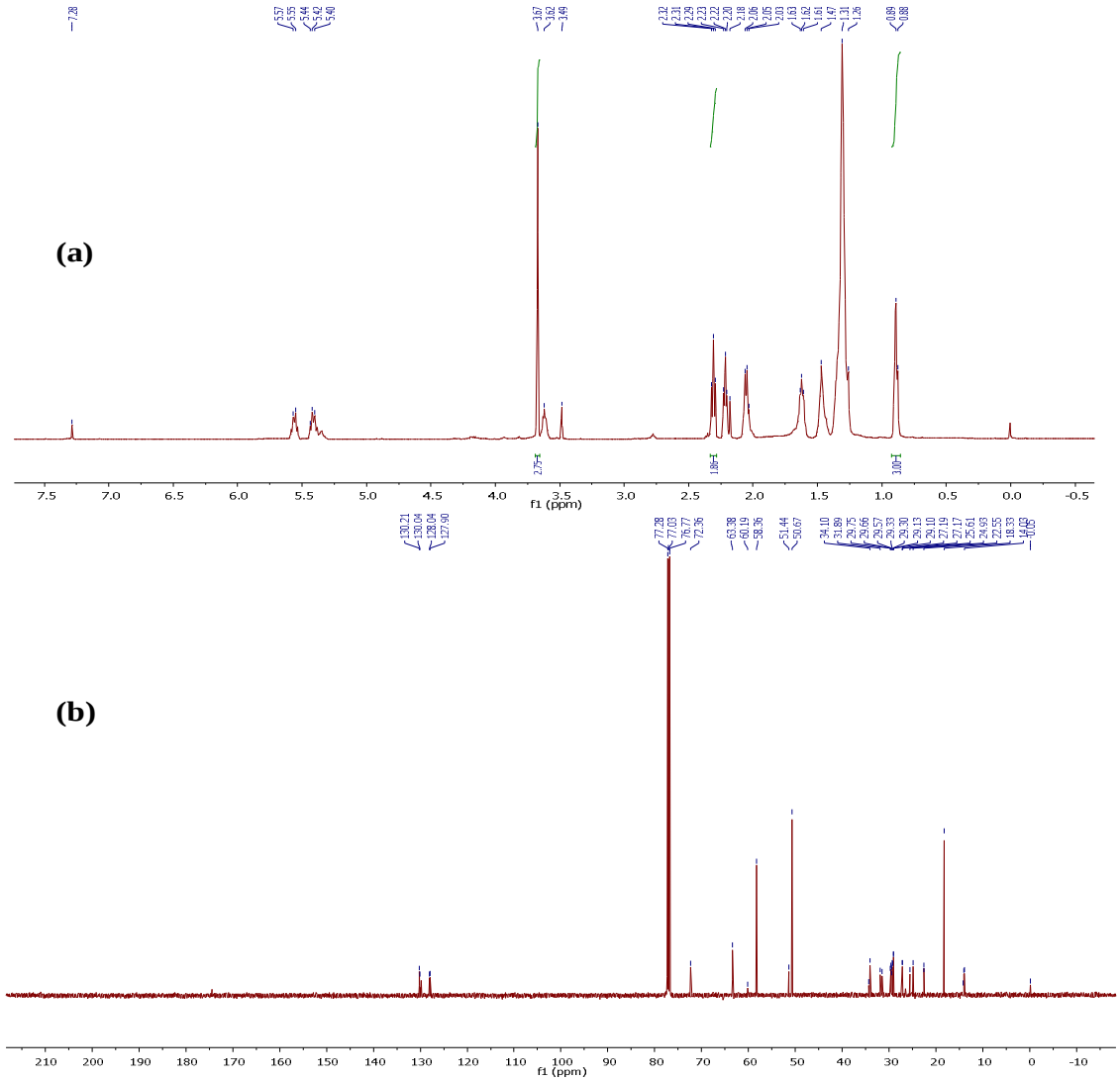

Figure 4.14 (a) ^{1}H-NMR spectra of fatty acid methyl ester obtained at most optimized condition of transesterification;(b) ^{13}C-NMR of methyl ester produced at optimized conditions of process of transesterification.

Additionally, a multiplet signal at δ 5.47-5.57 ppm was attributable to olefinic hydrogen present in FAME, respectively **(**Banerjee et al., 2019). Figure 4.14(b) illustrated the ^{13}C-NMR spectrum of fatty acid methyl ester from *Milletia pinnatta* oil. The signal of carbonyl carbon of methyl ester (-COOMe) in methyl ester emerged at 174.58ppm while methoxy carbon in FAME appeared at 51.69 ppm. The high intensity signals at 127.90-130.21ppm confirmed the unsaturation due to oleic acid methyl esters present in biodiesel corroborating the inference from GC-MS. The number of signals at

14 ppm and 22-34 ppm appeared because of carbons of terminal methyl groups and methylene group of long carbon chain in FAME.

4.9.3. ATR FT-IR

ATR FT-IR spectra (Figure 4.15) informs about all the necessary functional moieties present in karanja oil methyl ester. The consecutive three peaks at 3003cm^{-1}, 2920 cm^{-1}, and 2863 cm^{-1} represent the stretching of -C=C-H, -C-H, and -C-H in aldehydic bonds respectively (Smith, 2016). The bending oscillations of methyl groups evolved at 1480 cm^{-1} and 1353 cm^{-1}, while methylene bending vibrations showed their presence at 1241cm^{-1} and 720 cm^{-1} (Smith, 2015). The characteristic peak of methoxy carbonyl group in biodiesel appeared at 1738 cm^{-1}. The C-O stretching vibration in biodiesel showed two asymmetric coupled vibrations at 1171 cm^{-1} and 1113 cm^{-1} due to (-C-CO-O-) and 1035 cm^{-1} due to (-O-C-C-) bonds (Smith, 2017). The methyl group stretching band appeared at 2923 cm^{-1}, while methylene stretching band at 2854 cm^{-1} (Smith, 2016; Smith, 2015). The out of plane bending of cis (-HC=CH-) showed its existence at 583cm^{-1} and 515cm^{-1} (Smith, 2015).

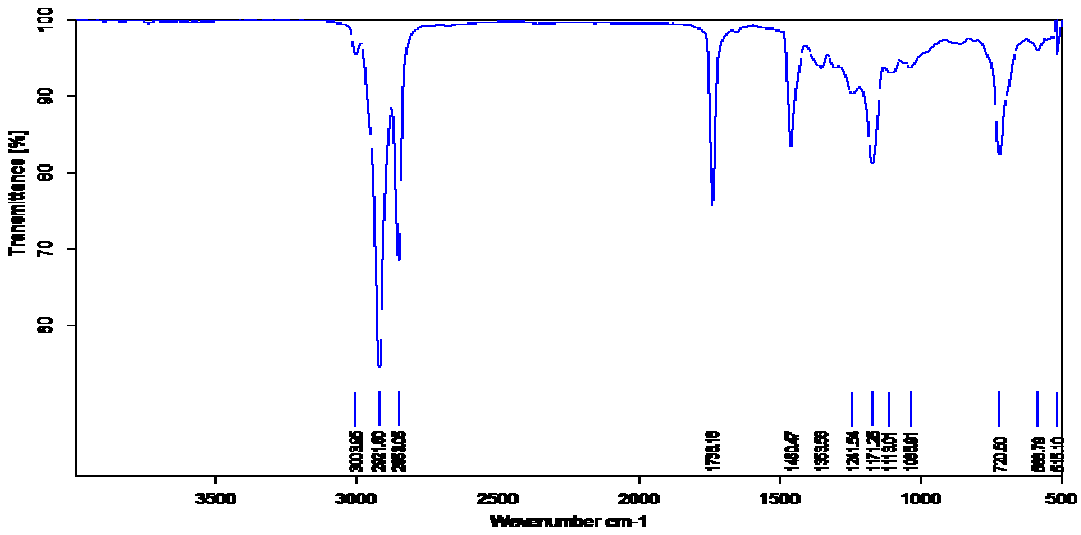

Figure 4.15 ATR FT-IR spectrum of fatty acid methyl ester derived from *Milletia pinnata* oil.

4.9.4. Investigation of physicochemical properties of methyl ester

The prepared KOME with the highest conversion underwent for physicochemical analysis to ensure its suitability for engines without modification. The several important physicochemical properties of raw karanja oil and FAME have been compared in Table 4.2. The transesterification reaction lessened the kinematic viscosity from 39.0 mm^2/s to 5.83 mm^2/s and density from 0.921g/cm^3 to 0.883 g/cm^3 which enabled it as fit as the conventional fuel. Fuel properties such as flash point and cloud point were also considerably reduced. Flash point of KOME was found to be 147°C which indicates that produced KOME was not susceptible for explosion at moderate temperature. Cloud point of KOME was also obtained to be quite low which makes KOME operative even in cold region. This had been found that KOME differed from karanja oil in various aspects and incorporated better qualities quite closer to that of ideal diesel fuel. This informs that the produced biodiesel is safer than the conventional fuel. Finally, the measured fuel properties of KOME ascertained the prepared biodiesel to be compatible with ASTM biodiesel standards (D6751a).

Table 4.2

Physicochemical properties of fatty acid methyl esters derived from *Milletia pinnata* oil.

Properties	**Unit**	***Milletia pinnata* oil.**	**FAME**	**ASTM standards**
Acid value	mg KOH/g	8.0	0.5	D664
Color	-	Yellowish red	Yellowish	Yellowish
Calorific value	(MJ/kg)	39.01	37.65	D4809
Copper strip corrosion	-	1a	1a	D130

Cetane number	-	38	55	D 613
Density (at 15˚C)	g/cm^3	0.921	0.883	D1298
Flash point	˚C	228	147	D93
Cloud point	˚C	2	-1	D93
Kinematic viscosity (at 40˚C)	mm^2/s	39	5.83	D445

4.10. Conclusions

Biodiesel was produced in laboratory by an economically viable transesterification reaction using a novel heterogeneous basic catalyst. The perovskite barium cerate was successfully prepared by sol-gel polymer precursor method. The desired structure was proved by PXRD, SEM, and FT-IR. Various Ba/Ce stoichiometric ratios were inspected for catalytic activity. Among all, perovskite barium cerate ($BaCeO_3$) was proved to be an active and stable catalyst for the methanolysis of karanja oil. The surface area analysis of $BaCeO_3$ was determined and its specific surface area (S_{BET}) was found to be $32m^2/g$, and its pore size distribution confirmed it as mesoporous material. The influence of various parameters such as catalyst dose, oil to alcohol molar ratio, reaction temperature, reaction time and agitation speed were thoroughly studied and the KOME with remarkable (98.4±0.4%) conversion was synthesized at optimum reaction conditions (catalyst dose;1.2 wt %, oil to methanol molar ratio;1:19, reaction temperature; 65˚C, reaction time;100 min, and agitation speed; 600 rpm. The reaction followed pseudo-first order kinetics. The activation energy (E_a) was 42.77kJ mol^{-1} and the frequency factor (A) to be $11.94\times10^4 min^{-1}$. Barium cerate has got the excellent reusability till sixth cycle with KOME conversion capacity greater than 81%. In present study, green chemistry metrics such as E-factor value of 0.088 illustrated $BaCeO_3$ catalysed transesterification reaction as a clean

production technique. TOF was also quantified as $21\times10^{-2}s^{-1}$ classifying the perovskite $BaCeO_3$ as efficient and sustainable catalyst for transesterification to produce biodiesel. The prepared KOME with the highest KOME conversion underwent for physicochemical analysis to assure its suitability for engines without modification. All the physicochemical properties accounted in this study were well within the permissible range prescribed by ASTM standards which approved the produced biodiesel a clean and efficient alternative for conventional diesel fuel.